The 3-dimensional structure of a hepatitis C virus p7 ion channel by electron microscopy

Philipp Luik[a], Chee Chew[b], Jussi Aittoniemi[b], Jason Chang[c], Paul Wentworth, Jr[c], Raymond A. Dwek[a], Philip C. Biggin[b], Catherine Vénien-Bryan[d], and Nicole Zitzmann[a,1]

Department of Biochemistry and [a]Oxford Glycobiology Institute, [b]Structural Bioinformatics and Computational Biochemistry, [c]The Scripps/Oxford Laboratory, and [d]Laboratory of Molecular Biophysics, University of Oxford, South Parks Road, Oxford OX1 3QU, United Kingdom

Communicated by Charles M. Rice, The Rockefeller University, New York, NY, May 29, 2009 (received for review December 23, 2008)

Infection with the hepatitis C virus (HCV) has a huge impact on global health putting more than 170 million people at risk of developing severe liver disease. The HCV encoded p7 ion channel is essential for the production of infectious viruses. Despite a growing body of functional data, little is known about the 3-dimensional (3D) structure of the channel. Here, we present the 3D structure of a full-length viroporin, the detergent-solubilized hexameric 42 kDa form of the HCV p7 ion channel, as determined by single-particle electron microscopy using the random conical tilting approach. The reconstruction of such a small protein complex was made possible by a combination of high-contrast staining, the symmetry, and the distinct structural features of the channel. The orientation of the p7 monomers within the density was established using immunolabeling with N and C termini specific F_{ab} fragments. The density map at a resolution of ≈16 Å reveals a flower-shaped protein architecture with protruding petals oriented toward the ER lumen. This broadest part of the channel presents a comparatively large surface area providing potential interaction sites for cellular and virally encoded ER resident proteins.

membrane protein | viroporin | single particle analysis | random conical tilt reconstruction

The hepatitis C virus (HCV) poses a major global health problem. It puts more than 170 million people worldwide at risk of developing liver cirrhosis and hepatocellular carcinoma. HCV comprises 6 different genotypes and is one of the fastest mutating viruses known to man. There is no vaccine available, and treatment options are genotype-specific, prone to viral escape mutations, and inadequate.

The HCV p7 ion channel is a more recent addition to the growing list of potential drug targets encoded by HCV, reflecting the urgent need for a therapeutic approach. p7 is critical for the release of infectious virions in vitro (1, 2) and in vivo (3). It is not involved in HCV RNA replication (4, 5), but is required for late steps of viral particle assembly (2) and potentially cell entry (6). However, the prerequisite incorporation of p7 into budding virions has not been demonstrated.

p7 belongs to the viroporins, small virally encoded proteins with at least 1 membrane-spanning helix that oligomerize to form channels or pores that modify the permeability of the cell membrane to ions and other small molecules (7). In planar lipid bilayers, p7 monomers oligomerize to form cation-selective ion channels that can be specifically inhibited by long alkylchain iminosugars, amiloride, and amantadine derivatives, with varying reported efficacies (6, 8–15). Each HCV p7 monomer consists of 63 aa, most of which are hydrophobic and possibly contain endoplasmic reticulum (ER) retention signals (16–18). Computational secondary structure predictions suggest that the monomers contain 2 transmembrane spanning helices connected by a short basic loop (19, 20). The loop is assumed to face the cytoplasm, with the N and C termini facing the ER lumen. Recent electrophysiological experiments suggest that the N-terminal helix lines the pore (15). Electron microscopy studies aimed at defining the oligomerization state of the p7 channel have suggested that monomers assemble into either hexamers (10) or heptamers (9) in lipid bilayers.

We report here the 3-dimensional (3D) structure of an HCV p7 ion channel. Chemically synthesized p7 monomers of native length and charge were solubilized in detergent. The resulting oligomeric channels were negatively stained, imaged, and analyzed using single particle reconstruction. The 3D structure was determined by the random conical tilt approach at a resolution of ≈16 Å. It reveals a conically shaped channel with protruding petals adopting hexameric symmetry under these experimental conditions. Immunoelectron microscopy experiments were used to determine the orientation of p7 monomers in the electron density, and computational models of p7 monomers were fitted into the 3D density map. The assembled channel structure will aid our understanding of its physiological function as an ion channel, as an interaction partner for virally and host cell encoded proteins, and as an antiviral drug target.

Results

Native Gel Electrophoresis and Chemical Cross-Linking. HCV p7 (strain JFH-1, genotype 2a) was chemically synthesized and purified to >95% by reverse phase high-performance liquid chromatography. The resulting peptides formed active ion channels in artificial membranes (15). For the current study, we dissolved p7 peptides in the mild detergent 1,2-diheptanoyl-*sn*-glycero-3-phosphocholine (DHPC) and determined their oligomerization state by blue native polyacrylamide gel electrophoresis (BN-PAGE), which allows proteins to maintain their undenatured native state and oligomerization pattern. Under these conditions, we detected no monomers and only 1 oligomerized p7 species (Fig. 1*A*). The homogeneity and monodispersity of the sample was confirmed by size exclusion chromatography of the DHPC solubilized p7 channel (Fig. S1). However, both techniques do not allow us to distinguish between p7 hexamers (42 kDa) and heptamers (49 kDa).

We performed cross-linking experiments using the homobifunctional cross-linker 1,11-bis(maleimido)triethylene glycol [$BM(PEO)_3$]. The 3 cysteine residues in the JHF-1 p7 peptide provide several possibilities for intermolecular reactions between sulfhydryl groups of adjacent p7 monomers forming a channel. Cross-linked peptides were separated by SDS-PAGE using untreated p7 as control (Fig. 1*B*). Reaction mixtures containing either 90 or 45 μM of p7 peptide resulted in 6 clearly visible bands on the gel, suggesting a hexameric oligomerization state. Interestingly, the untreated control resulted in the appearance of 2 bands. The presence of a high concentration of

Author contributions: P.L. and N.Z. designed research; P.L., C.C., J.A., J.C., P.W., and C.V.-B. performed research; P.L., C.C., J.A., R.A.D., P.C.B., C.V.-B., and N.Z. analyzed data; and P.L. and N.Z. wrote the paper.

The authors declare no conflict of interest.

See Commentary on page 12567.

[1]To whom correspondence should be addressed. E-mail: nicole.zitzmann@bioch.ox.ac.uk.

This article contains supporting information online at www.pnas.org/cgi/content/full/0905966106/DCSupplemental.

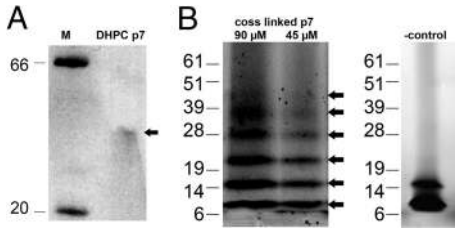

Fig. 1. BN-PAGE analysis and chemical cross-linking of HCV p7 oligomers. (*A*) BN-PAGE analysis of DHPC solubilized HCV p7 (JFH-1 strain, genotype 2a) oligomers (DHPC p7). The single oligomerized p7 species detected in the DHPC solubilized sample is indicated by an arrow and most likely represents the hexamer (42 kDa); M, marker. (*B*) SDS-PAGE analysis of cross-linked DHPC-solubilized p7 oligomers (90 and 45 μM). The arrows indicate bands corresponding to the monomer, dimer, trimer, tetramer, pentamer, and hexamer, respectively. The negative control without the BM(PEO)$_3$ cross-linking agent (-control) shows monomeric and dimeric species.

reducing agent (100 mM β-mercaptoethanol) in the SDS sample buffer makes an intermolecular disulfide bond unlikely. However, the reduction of disulfide bonds in a hydrophobic environment is particularly difficult, and the existence of such bonds cannot be ruled out. Alternatively, a strong hydrophobic interaction between 2 p7 monomers could be responsible for forming dimers that are not disrupted by the SDS in the loading buffer and in the gel.

Electron Microscopy of HCV p7 Hexamers. In negative stain electron microscopy images, DHPC-solubilized p7 hexamers were monodispersed and homogeneous in size (5–9 nm) with the exception of a few large protein aggregates (Fig. 2*A*). We identified 2 major particle shapes, a triangular and a circular shape, corresponding to the side and top view of the p7 channel, respectively.

To calculate 3D maps, we recorded image pairs at the same location of the specimens at 50° tilt and 0°. The images of untilted specimens were used to classify the particles according to their shape, and the images of the tilted specimens were used to calculate 3D reconstructions of individual classes using the random conical tilt approach (21).

In brief, 1,761 pairs of tilted and untilted particles were classified into 20 classes using multivariate statistical analysis and multi-reference alignment (22). For each class, an initial 3D model was built, and 7 classes were merged into 1 starting volume. This volume was further refined using 8,698 additional particles in 5 cycles. The hexameric symmetry suggested by the cross-linking experiments was confirmed by harmonic analyses of the "top-view" class averages (Figs. S2 and S3). Therefore, a 6-fold symmetry was applied, and refinement was continued until no further improvement was achieved. As a control, penta- and heptameric symmetries were also applied, but did not result in equally well-resolved structures. Particle views are well distributed over all Euler angles (Fig. 2*B*) providing the basis for a reliable reconstruction. The resolution of the final 3D structure was calculated at ≈16 Å (Fig. 2*C*) using the FSC = 0.5 criterion of the Fourier shell correlation technique (23).

Re-projections from the density maps (Fig. 2*D Upper*) are very similar to the class averages (Fig. 2*D Lower*), indicating the consistency of the 3D reconstructions with the projections. The 6-fold symmetry was supported by class-averaged images of particles seen from the top (see also Fig. S4).

The p7 hexamer has a flower-like shape with 6 distinctive petals (Fig. 3). The petals branch off from a compact base with a tilt angle of up to 40°, forming a kink at approximately half the height of the channel. This results in a channel complex diameter of 8.1 nm at its broadest point in the top half and 3.2 nm at its narrowest toward the bottom. The entire channel complex is 4.8

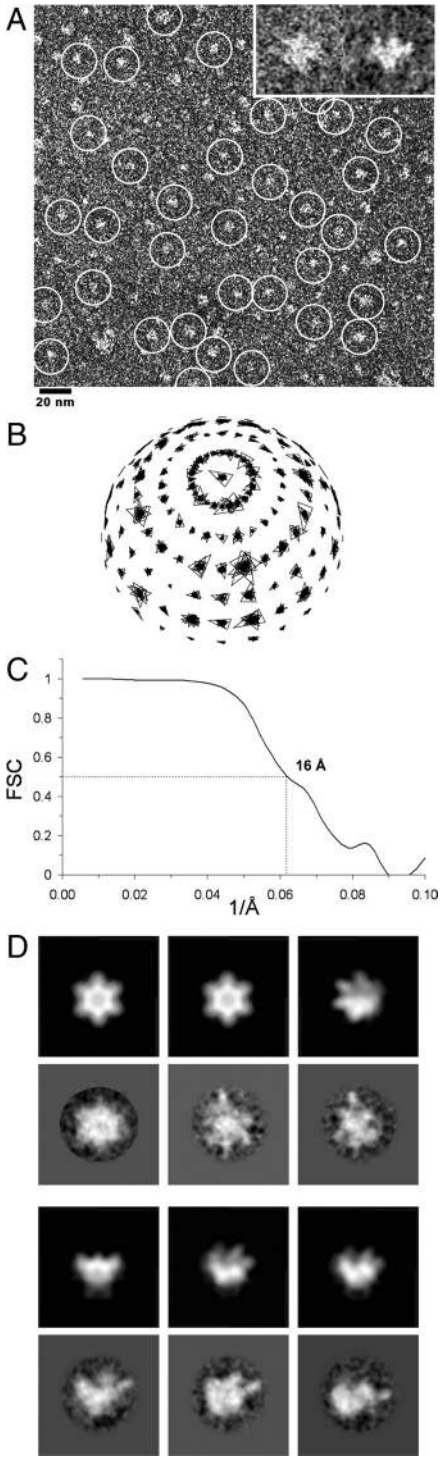

Fig. 2. Single particle electron microscopy of the HCV p7 channel. (*A*) Typical view from a raw image of p7 oligomers negatively stained with PTA at low magnification. A randomly selected subset of individual p7 particles are highlighted with white circles. Shown in the top right corner are a typical top view and a typical side view of selected single particles. (*B*) Plot of the Euler angle distribution using Xmipp (36). The topological sphere shows the angular distribution of the particles. Particles are distributed evenly across the whole sphere and contribute from all orientations to the 3D reconstruction. Larger triangles denote a larger number of particles. (*C*) Determination of the resolution of the final 3D reconstruction. The Fourier shell correlation (FSC) suggests a resolution of 16 Å using the 0.5 criterion. (*D*) Gallery of 6 representative class averages (*Lower*) of the untilted particle set compared with projections of the final 3D volume (*Upper*). The hexameric symmetry, petal features, and conical shape can be distinguished.

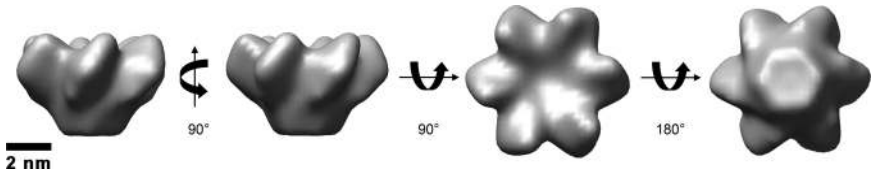

Fig. 3. The 3D structure of a hexameric HCV p7 channel. Views of the final 3D volumes of the HCV p7 channel filtered at 16 Å. The density threshold was set to 4 sigma. The cone-shaped structure is 8.1 nm in diameter at the widest point and 4.8 nm in height. Six protrusions or petals branch off a solid base resulting in a wide pore at the top of the channel.

nm in height; the petals—viewed from the top—have a diameter of ≈2.0 nm. The reconstructed volume is 89.4 kDa in mass calculated with a standard protein density of 0.84 DaÅ^{-3}. This corresponds to 2.1 times the expected molecular mass of the hexameric volume of the p7 channel (42 kDa). The larger size may be due to a thick layer of detergents binding to the channel and/or staining effects from the negative stain grains.

Immunoelectron Microscopy of the p7 Oligomers. p7 channels from single particle analysis were analyzed by immuno-EM using N and C terminus-specific F_{ab} fragments derived from p7 specific antibodies. The rectangular shapes of the F_{ab} fragments could be readily distinguished from the triangular p7 side views in the F_{ab}-p7 complexes (Fig. 4). The staining pattern indicates that both termini are located at the wide top of the channel, presumably in the petals of the p7 volume. This determined the p7 monomer orientation within the oligomeric p7 volume for subsequent modeling.

Molecular Dynamics Simulation and Model Fitting. Coarse-grained molecular dynamics (CGMD) simulations of p7 monomers in self-assembled bilayers consisting of 1-palmitoyl-2-oleoyl-*sn*-glycero-3-phosphoethanolamine (POPE) and 1-palmitoyl-2-oleoyl-*sn*-glycero-3-phosphocholine (POPC), at a ratio of 4:1, indicate that p7 monomers adopt a predominantly α-helical hairpin topology. Cluster analysis was performed on the CGMD structures and resulted in the generation of a single CG p7 hairpin model. The CG model was converted into an atomistic model. Six of the atomistic models were then modeled into the 3D density volume with the N-terminal transmembrane helices lining the inner channel pore (15). The p7 monomers were fitted into the petals guided by the results from the immunolabeling with both the N and C termini located at the petal tips (Fig. 5). This fit resulted in a fitting value of 97.3% of modeled atoms located within the EM density volume, with most contacts between monomers found in the closely packed lower part of the helix bundle. The fact that the reconstructed volume is bigger than the actual protein mass contributes to the high fitting value.

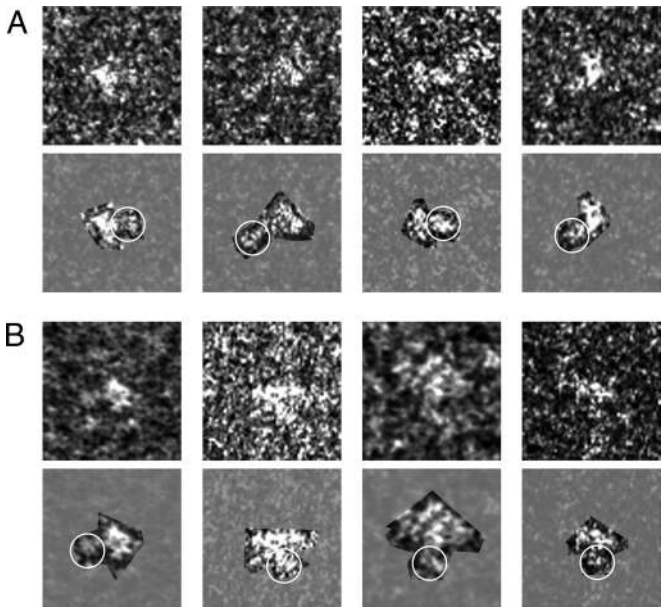

Fig. 4. Immunoelectron microscopy of the p7 channel. Electron microscopy images of p7 channels in complex with anti-C terminus (*A*) and anti-N terminus (*B*) F_{ab} -fragments. Each panel shows duplicates of the same image, with raw data at the top, and highlighted complexes with F_{ab} fragments bound (white circle) at the bottom. Both N and C termini specific F_{ab}-fragments bind to the open ''top'' part of the channel, where the petals are located.

Discussion

In our study we obtained the structure of an entire viroporin. Previously, the tetrameric structure of the transmembrane domains of the influenza A virus encoded viroporin M2 has been solved to atomic resolution using NMR (24) and X-ray crystallography (25). However, the complete structure encompassing the entire protein is still missing.

For the p7 channel, the protein content accounts for 42 kDa; the estimated mass of the negatively stained detergent surrounded complex was ≈90 kDa. Together with the recently published 3D reconstruction of the adiponectin trimer, which has a total molecular mass of ≈80 kDa (26), the HCV p7 ion channel is one of the smallest sized objects to be visualized by single particle image analysis to date. The single particle reconstruction of a channel complex comprising 6 chemically synthesized p7 monomers of native size (63 aa) and charge (pI 8.8) represents a proof of principle demonstration that the 3D structure of very small complexes can be determined although they may be difficult to visualize, align, and classify. Among the factors contributing to the successful imaging were the high contrast achieved by phosphotungstic acid (PTA) staining, the conical shape with very distinct protrusions adopted by the channel, and its symmetry.

p7 oligomerization has been investigated in 2 previous studies by Griffin et al. (10) and Clarke et al. (9). In both studies, di-thio-bis-succinimidyl proprionate (DSP) was used as cross-linking agent. The hexahis-p7 (10) and FLAG-p7 (9) were reported to form hexa- and heptamers, respectively, in a unilamellar lipid environment.

Here, we use 1,11-bis(maleimido)triethylene glycol, BM-$(PEO)_3$, as cross-linking agent for native p7 and detect hexameric channel complexes in a detergent environment.

The study using hexahis-p7 arrived at a diameter value of 5.4 nm for the p7 part of the tagged protein complex (10). GST-FLAG-tagged p7 formed heptamers in lipid bilayers with an estimated diameter of 10 nm of the entire tagged complex (9). Our measurements yield an overall diameter ranging from 3.2 nm at the narrowest to 8.1 nm at the widest for the conically shaped untagged hexamer. The discrepancy in diameter measurements between the different studies may originate from a combination of factors including the absence/presence of protein tags, the use of p7 derived from different genotypes, and

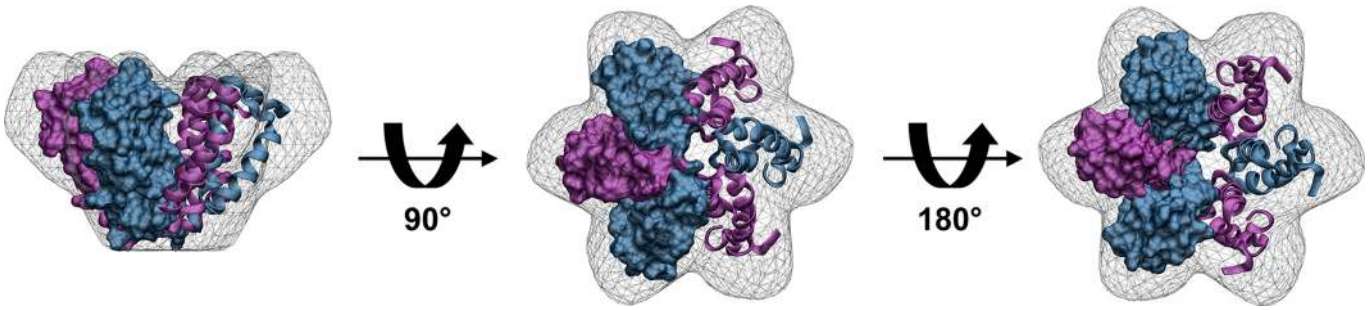

Fig. 5. Fitting of simulated p7 monomers into the hexameric volume. Atomistic models of p7 monomers were fitted into the EM density with their C and N termini oriented toward the petal tips. For illustration purposes, alternating colors of the monomers (blue and purple) were chosen. In each model, 3 neighboring monomers are surface represented; for the other 3, the peptide backbones are shown.

detergent versus lipid environment. Although DHPC is a mild detergent resembling phospholipids, p7 may well oligomerize differently in this environment compared with that of a lipid bilayer. We do not rule out the existence of a heptamer or coexistance of hexa- and heptamers under other conditions.

Inspection of our structure, which is resolved at ≈16 Å, suggests that direct contacts between p7 monomers will be restricted to the "bottom" half of the channel. We were able to assign the correct orientation of the alpha helices by immunolabeling of the hexamers. Both termini face toward the petals at the "top" of the channel. Therefore, we can conclude that this broader top is oriented toward the ER lumen. There is a strong tilt angle of the density map observed at approximately half the channel's height. This structure shows that a much larger exposed surface area provided by the open petals may be available for interactions with host or viral proteins than could be assumed based on computer models alone (10, 20). This accessible area faces the interior of the ER, and potential interaction partners would have to share this location.

In conclusion, our study has provided the 3D visualization that may help gain detailed molecular insight into the various proposed roles of the p7 complex as an ion channel and as interaction partner for virally encoded and host cell proteins. p7 has been identified as a promising future drug target in the fight against HCV infection, and our study may provide a framework for the rational design of therapeutics.

Materials and Methods

Peptide Synthesis. HCV p7 (strain JFH-1, genotype 2a, accession number: AB047639) was chemically synthesized and reverse phase high-performance liquid chromatography purified to >95% (15). Its identity was confirmed by mass spectrometric analysis, and its ion channel functionality demonstrated (15).

BN-PAGE of Native p7 and SDS-PAGE Analysis of Chemically Cross-Linked p7. For BN-PAGE analysis of native p7, the published method (27–29) was optimized. Briefly, 1 μL of a 1 mg/mL p7 stock solution in 50 mM 1,2-diheptanoyl-*sn*-glycero-3-phosphocholine (DHPC) (Avanti Polar Lipids) was adjusted to a total volume of 20 μL using protein sample buffer [50 mM Bis-Tris, pH 7.2, 0.016 N HCl, 50 mM NaCl, 10% (wt/vol) glycerol, 0.001% Ponceau S, 0.5% Coomassie G-250 sample additive; Invitrogen] and a final concentration of 15 mM DHPC. The sample was run on 5–18% acrylamid linear gradient gels containing 50 mM Bis-Tris and 0.5 M ε-aminocaproic acid, pH 7.0. The anode buffer contained 50 mM Bis-Tris, 50 mM tricine, pH 6.8, and the cathode buffer contained 50 mM Bis-Tris, 50 mM tricine, and 0.02% (wt/vol) Coomassie brilliant blue (CBB) G-250, pH 6.8. Gels were run for 1 h at 150 V and room temperature, then the cathode buffer was replaced by a buffer containing 0.002% (wt/vol) CBB, and the run was continued until the dye front reached the bottom of the gel. Gels were stained with CBB R-250.

Cross-linking experiments were performed with 1,11-bis(maleimido)triethylene glycol, $BM(PEO)_3$ [28 mM stock solution in dimethyl sulfoxide (DMSO)], spacer arm length 17.8 Å (Pierce), which conjugates sulfhydryl groups (-SH) of the p7 channel. For cross-linking reactions, 2.5 μL $BM(PEO)_3$ stock solution was added to 20 μL of either a 90 μM or 45 μM p7 solution in 20 mM Hepes, pH 7.0, 15 mM NaCl, 5 mM EDTA, 5 mM DHPC, and the reaction mix was incubated at 4 °C for 2 h. Samples were quenched with 100 mM β-mercaptoethanol, and cross-linked proteins were separated by 4–16% (wt/vol) SDS-PAGE gradient gels under reducing conditions followed by staining with the fluorescent dye OGT 1238 (Oxford Glycosciences), as described in ref. 30. Gels were imaged on an Apollo II laser scanner (Oxford Glycosciences).

Electron Microscopy. For structural analysis, 3 μL of a 5 μg/mL p7 protein solution in 100 mM NaCl, 50 mM DHPC, 25 mM Hepes, pH 7.0, was applied to a hydrophilic glow discharged copper grid coated with a thin carbon film. Grids were washed with 2 drops of water to remove excess detergents, blotted with filter paper, negatively stained with 2% (wt/vol) phosphotungstic acid (PTA), and air-dried. Because of the very small size of the p7 complex, several different stains were tested before PTA was chosen because of the small grain size of the stain and the good contrast obtained. For instance, the complex was hardly visible using uranyl acetate (2%) or uranyl formate (0.75%). Micrographs were recorded on Kodak SO 163 film using a Philips CM120 electron microscope equipped with a LaB6 filament (FEI) operating at 120 kV under low dose conditions with a magnification of 45,000×. For random conical tilt reconstruction, pairs of images of the same specimen area were taken at tilt angles of 50° and 0°, respectively. An additional set of untilted images was taken for model refinement. Typically, defocus values were 800 nm for untilted images and 400–1,200 nm for tilted images.

Micrographs were digitized with a Super Coolscan 9000 ED (Nikon) using a step size of 12.5 μm, resulting in a pixel size of 2.78 Å for the specimen.

Image Analysis. All image processing was performed using the SPIDER/WEB software packages (31). Before the start of the random conical tilt reconstruction, 16,551 particles were picked from untilted images and windowed into 64 × 64-pixel boxes. All particles were visually inspected. Particles that either formed too large aggregates were overstained or had a very low contrast were rejected. For subsequent analysis 8,698 particles were finally selected. The particles were subjected to translational and rotational alignment and classified into 20 classes using principal component analysis (PCA) and K-mean clustering, which were used as references for subsequent multi-reference alignment (22). Multi-reference aligned particles were classified using PCA and K-means clustering into 20 output classes. Because of the small particle size, the alignment and classification method had to be extensively optimized. This was made possible by the characteristic shape of the particles, their symmetry, and the high-contrast staining.

For random conical tilt 3D reconstruction (21) of the p7 oligomer, all 1,761 pairs of particles were simultaneously selected from the tilted and untilted images, windowed, and used for the reconstruction of the initial volume. The untilted particle set was centered, aligned, and classified using the optimized method. The corresponding particles of the tilted image set were centered using cross-correlation and back-projected into 20 volumes. The volumes were compared by their cross-correlation coefficient, and 7 of these 20 classes (603 particles in total) were finally combined and used for 3D reconstruction of a reference volume. From this initial model, 3,248 back-projections with an increment of 2.5° were computed and subjected to refinement using the 1,761 tilted particles in 2 rounds of refinement.

For subsequent refinement, the 8,698 particles from the untilted particle set were used for 3 rounds of further refinement of the 3D volume. Because the resulting structure was clearly hexameric, which had also been observed in the class averages and in the cross-linking experiments, a 6-fold symmetry

was applied, and refinement was continued until no further improvement was achieved. The resolution of the final 3D structure was calculated at ≈16 Å using the FSC = 0.5 criterion of the Fourier shell correlation technique (23), and the structure was filtered to this value.

Immunoelectron Microscopy. F_{ab} fragments were generated from antibodies 2716 and 2717 (a kind gift from Dr. Steve Griffin, University of Leeds, UK), which are directed against the N and C termini of JFH-1 p7, respectively (6). Twenty micrograms of both full-length antibodies were dialyzed in 30 μL against F_{ab} digestion buffer (Pierce) and digested individually for 4 h shaking at 800 rpm, 37 °C, on an agarose column with immobilized papain (Pierce). Digested sample was eluted by centrifugation, and Fc fragments as well as undigested antibodies were removed using NAb Protein A spin columns (Pierce).

A 3.5-μg/mL p7 protein solution was prepared in 100 mM NaCl, 1.5% (wt/vol) DHPC, 40 mM Hepes, pH 7.0. Two microliters p7 solution were added to 6 μL of 2716 and 2717 anti-p7 F_{ab} fragment solutions, respectively, incubated for 1 h, and subsequently applied onto an electron microscopy grid. Micrographs were generated and processed as described above.

Molecular Dynamics Simulation and Model Fitting. A coarse grain (CG) model of HCV JHF-1 p7 was built according to consensus secondary structure prediction and simulated in a self-assembled lipid bilayer (full description of the CG simulation can be found in the *SI Text*).

Hairpin structures of all CG simulations (5 × 2 μs) were clustered. The most representative CG monomer was converted into atomistic detail using the software Modeller v8 (http://www.salilab.org/modeller/), by using the positions of the CG backbone particles as templates for the positions of the alpha carbons (32, 33). To obtain the best fitted atomistic model, we generated 1,000 atomistic models from the CG model, which were then filtered using the root mean square deviation of the backbone positions. Six identical copies of the resulting monomer were manually fitted to form a symmetric hexamer (by rotation around the symmetry axis). This hexamer was subsequently refitted into the EM density by rigid body docking using Chimera (34). Images were generated using Visual Molecular Dynamics (35).

ACKNOWLEDGMENTS. We thank Dr. R. Antrobus for mass spectrometric analysis and Dr. C. Fotinou for help with the gel filtration experiment. The work was supported by the Oxford Glycobiology Institute Endowment. P.L. is funded by a Pfizer Royalties Scholarship, and C.C. and J.A. by Wellcome Trust Studentships. P.C.B is a Research Councils United Kingdom fellow. C.V.B. is funded by the Wellcome Trust. N.Z. is a Glycobiology Career Development Fellow and Senior Research Fellow of Linacre College, Oxford.

1. Jones CT, Murray CL, Eastman DK, Tassello J, Rice CM (2007) Hepatitis C virus p7 and NS2 proteins are essential for production of infectious virus. *J Virol* 81:8374–8383.
2. Steinmann E, et al. (2007) Hepatitis C virus p7 protein is crucial for assembly and release of infectious virions. *PLoS Pathog* 3:e103.
3. Sakai A, et al. (2003) The p7 polypeptide of hepatitis C virus is critical for infectivity and contains functionally important genotype-specific sequences. *Proc Natl Acad Sci USA* 100:11646–11651.
4. Blight KJ, McKeating JA, Rice CM (2002) Highly permissive cell lines for subgenomic and genomic hepatitis C virus RNA replication. *J Virol* 76:13001–13014.
5. Lohmann V, et al. (1999) Replication of subgenomic hepatitis C virus RNAs in a hepatoma cell line. *Science* 285:110–113.
6. Griffin S, et al. (2008) Genotype-dependent sensitivity of hepatitis C virus to inhibitors of the p7 ion channel. *Hepatology* 48:1779–1790.
7. Gonzalez ME, Carrasco L (2003) Viroporins. *FEBS Lett* 552:28–34.
8. Steinmann E, et al. (2007) Antiviral effects of amantadine and iminosugar derivatives against hepatitis C virus. *Hepatology* 46:330–338.
9. Clarke D, et al. (2006) Evidence for the formation of a heptameric ion channel complex by the hepatitis C virus p7 protein in vitro. *J Biol Chem* 281:37057–37068.
10. Griffin SD, et al. (2003) The p7 protein of hepatitis C virus forms an ion channel that is blocked by the antiviral drug, Amantadine. *FEBS Lett* 535:34–38.
11. Pavlovic D, et al. (2003) The hepatitis C virus p7 protein forms an ion channel that is inhibited by long-alkyl-chain iminosugar derivatives. *Proc Natl Acad Sci USA* 100:6104–6108.
12. Premkumar A, Wilson L, Ewart GD, Gage PW (2004) Cation-selective ion channels formed by p7 of hepatitis C virus are blocked by hexamethylene amiloride. *FEBS Lett* 557:99–103.
13. St Gelais C, et al. (2007) Inhibition of hepatitis C virus p7 membrane channels in a liposome-based assay system. *Antiviral Res* 76:48–58.
14. Griffin SD, et al. (2004) A conserved basic loop in hepatitis C virus p7 protein is required for amantadine-sensitive ion channel activity in mammalian cells but is dispensable for localization to mitochondria. *J Gen Virol* 85:451–461.
15. Chew CF, Vijayan R, Chang J, Zitzmann N, Biggin PC (2009) Determination of pore-lining residues in the hepatitis C virus p7 protein. *Biophys J* 96:L10–L12.
16. Lin C, Lindenbach BD, Pragai BM, McCourt DW, Rice CM (1994) Processing in the hepatitis C virus E2-NS2 region: Identification of p7 and two distinct E2-specific products with different C termini. *J Virol* 68:5063–5073.
17. Griffin SD, Clarke D, McCormick C, Rowlands D, Harris M (2005) Signal peptide cleavage and internal targeting signals direct the hepatitis C virus p7 protein to distinct intracellular membranes. *J Virol* 79:15525–15536.
18. Haqshenas G, Mackenzie JM, Dong X, Gowans EJ (2007) Hepatitis C virus p7 protein is localized in the endoplasmic reticulum when it is encoded by a replication-competent genome. *J Gen Virol* 88:134–142.
19. Carrere-Kremer S, et al. (2002) Subcellular localization and topology of the p7 polypeptide of hepatitis C virus. *J Virol* 76:3720–3730.
20. Patargias G, Zitzmann N, Dwek R, Fischer WB (2006) Protein–protein interactions: Modeling the hepatitis C virus ion channel p7. *J Med Chem* 49:648–655.
21. Radermacher MM, Wagenknecht T, Verschoor A, Frank J (1987) Three-dimensional reconstruction from a single-exposure, random conical tilt series applied to the 50S ribosomal subunit of *Escherichia coli*. *J Microsc* 146:113–136.
22. van Heel M, Stöffler-Meilicke M (1985) Characteristic views of *E. coli* and *B. stearothermophilus* 30S ribosomal subunits in the electron microscope. *EMBO J* 4:2389–2395.
23. van Heel M (1987) Similarity measures between images. *Ultramicroscopy* 21:95–100.
24. Schnell JR, Chou JJ (2008) Structure and mechanism of the M2 proton channel of influenza A virus. *Nature* 451:591–595.
25. Stouffer AL, et al. (2008) Structural basis for the function and inhibition of an influenza virus proton channel. *Nature* 451:596–599.
26. Radjainia M, Wang Y, Mitra AK (2008) Structural polymorphism of oligomeric adiponectin visualized by electron microscopy. *J Mol Biol* 381:419–430.
27. Schägger H (2001) Blue-native gels to isolate protein complexes from mitochondria. *Methods Cell Biol* 65:231–244.
28. Schägger H, Cramer WA, von Jagow G (1994) Analysis of molecular masses and oligomeric states of protein complexes by blue native electrophoresis and isolation of membrane protein complexes by two-dimensional native electrophoresis. *Anal Biochem* 217:220–230.
29. Schägger H, von Jagow G (1991) Blue native electrophoresis for isolation of membrane protein complexes in enzymatically active form. *Anal Biochem* 199:223–231.
30. Garcia A, et al. (2004) Differential proteome analysis of TRAP-activated platelets: Involvement of DOK-2 and phosphorylation of RGS proteins. *Blood* 103:2088–2095.
31. Frank J, et al. (1996) SPIDER and WEB: Processing and visualization of images in 3D electron microscopy and related fields. *J Struct Biol* 116:190–199.
32. Carpenter T, Bond PJ, Khalid S, Sansom MS (2008) Self-assembly of a simple membrane protein: Coarse-grained molecular dynamics simulations of the influenza M2 channel. *Biophys J* 95:3790–3801.
33. Wee CL, Balali-Mood K, Gavaghan D, Sansom MS (2008) The interaction of phospholipase A2 with a phospholipid bilayer: Coarse-grained molecular dynamics simulations. *Biophys J* 95:1649–1657.
34. Pettersen EF, et al. (2004) UCSF Chimera: A visualization system for exploratory research and analysis. *J Comput Chem* 25:1605–1612.
35. Humphrey W, Dalke A, Schulten K (1996) VMD: Visual molecular dynamics. *J Mol Graphics* 14:33–38;27–28.
36. Sorzano COS, et al. (2004) XMIPP: A new generation of an open-source image processing package for electron microscopy. *J Struct Biol* 148:194–204.